

Mississippi State University

Scholars Junction

College of Arts and Sciences Publications and
Scholarship

College of Arts and Sciences

1994

Initiation and Study of Localized Corrosion by Scanning Electrochemical Microscopy

David O. Wipf

Mississippi State University, dow1@msstate.edu

Follow this and additional works at: <https://scholarsjunction.msstate.edu/cas-publications>



Part of the [Analytical Chemistry Commons](#), and the [Materials Chemistry Commons](#)

Recommended Citation

Wipf, David O., "Initiation and Study of Localized Corrosion by Scanning Electrochemical Microscopy" (1994). *College of Arts and Sciences Publications and Scholarship*. 27.

<https://scholarsjunction.msstate.edu/cas-publications/27>

This Preprint is brought to you for free and open access by the College of Arts and Sciences at Scholars Junction. It has been accepted for inclusion in College of Arts and Sciences Publications and Scholarship by an authorized administrator of Scholars Junction. For more information, please contact scholcomm@msstate.libanswers.com.

Initiation and Study of Localized Corrosion by Scanning Electrochemical Microscopy.

David O. Wipf

Department of Chemistry

Mississippi State University

Mississippi State MS 39762

This Postprint was published
David O. Wipf, *Colloids and Surfaces A: Physicochemical and Engineering Aspects*,
93, 1994, 251-261.

[https://doi.org/10.1016/0927-7757\(94\)02872-9](https://doi.org/10.1016/0927-7757(94)02872-9)



This work is licensed under a [Creative Commons Attribution-NonCommercial 4.0 International](https://creativecommons.org/licenses/by-nc/4.0/)

Abstract:

This paper describes methods to study the initiation and formation of localized corrosion pits on stainless-steel and aluminum samples. These methods are based on the use of a scanned probe microscope, the scanning electrochemical microscope (SECM). The SECM is specifically designed for operation in electrolyte solution and so is uniquely suited for examination of corrosion processes. SECM imaging of a corrosion pit on stainless steel is presented. In addition, the initiation of single pits on aluminum and stainless steel by using the SECM tip to electrogenerate a local source of Cl^- is described.

Revised: February 15, 1994

Because of the enormous economic loss and the safety problems corrosion causes, it has been extensively studied in order to minimize its effects and prevent its occurrence [1]. Despite this, much remains to be understood about the initiation, formation, and propagation of corrosion on metal and metallic alloy surfaces. Passive metals, such as stainless steel and aluminum, are normally protected from generalized corrosion by the presence of a thin passivating film composed of variously hydrated metal oxides. In the presence of chloride, bromide, or other "aggressive" ions, the passive film can undergo localized breakdown, resulting in accelerated pitting-type corrosion at these locations.

The dynamics of passive film breakdown and pit formation and initiation have been extensively studied [2–4]. Conventional electrochemical techniques, such as galvanostatic and potentiodynamic methods [5–6] have been used. Stochastic models have been used to statistically analyze the current or potential fluctuations due to pit nucleation [7–8]. The models are then used to predict rates of pit initiation and repassivation as well as induction times for pit formation. Several in-situ types of measurements have also been made. The most common of these is a scanning micro-reference electrode [9]. An improved version of this technique is the scanning vibrating electrode technique, SVET [10]. This method rasters a vibrating metal tip across a substrate in order to map the electric field generated near a corrosion site. Unfortunately, the resolution of these methods are rather low, with a resolved feature size of about 50 μm . Ultramicroelectrodes that are made from the metal under study have also been useful for the examination of corrosion [11]. Because of their small size, high time resolution can be achieved, allowing observation of corrosion processes occurring at the microsecond level. In addition, nucleation of single pits is the predominant occurrence, simplifying analysis.

In this paper, I demonstrate that the scanning electrochemical microscope (SECM) can be useful as a new method for the examination of corrosion processes. The SECM is a scanned-probe microscopes related to the scanning tunneling [12] and atomic force microscope [13] but is specifically designed as an in-situ probe of the surface of materials that are immersed in electrolyte solution (cf. Figure 1).

There are two general modes of operation of the SECM. In one form of operation, called the feedback mode, the SECM uses a mediator molecule and the faradaic current that flows from the electrolysis of the mediator at a small electrode tip (1 to 10 μm dia.) as a probe of a substrate surface [14–

16]. As the tip is brought close to the surface, the current flow due to the mediator electrolysis is perturbed in a manner that is characteristic for electronically insulating or conducting surfaces. At conducting surfaces the mediator can be restored to its original oxidation state by electron-transfer from the conducting substrate (Figure 2A). This leads to an increase in current due to a recycling of the mediator in the tip–surface gap and, thus, the current increases as the gap width decreases. At insulating surfaces, the tip current decreases with a decrease in gap width because the surface physically blocks the diffusion of mediator molecules to the tip electrode (Figure 2B). Thus, the SECM can image electronically insulating and conducting surfaces simultaneously. To image a surface with the SECM, the tip is brought to within a distance of about a tip diameter to the substrate surface and then the tip is scanned across the surface in a raster pattern. The variations in current flow with changes in tip–substrate height or substrate conductivity are plotted versus the tip position to generate a map of the surface height or conductivity.

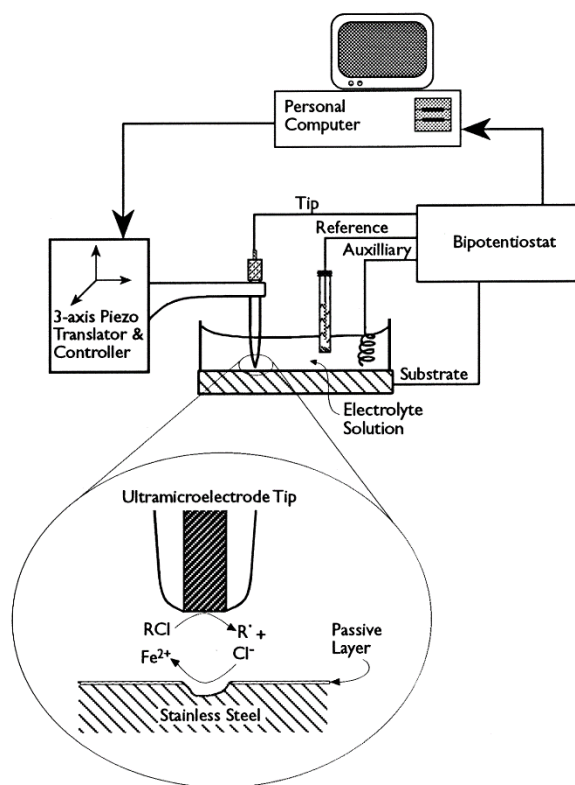


Figure 1. Schematic diagram of the scanning electrochemical microscope showing the pitting corrosion initiation process via Cl^- generation.

The other general mode of operation of the SECM is known as the generation/collection, g/c, mode. In this mode, the tip is polarized to electrolyze species in solution. If these species are generated by the substrate, a map can be made of their concentration distribution in solution by monitoring the current generated by their electrolysis as a function of tip position (Figure 2C). Although the g/c mode is less sensitive to surface topography and surface conductivity than the feedback mode, the g/c mode does not require the addition of an external mediator. More importantly, in the g/c mode the SECM tip can be used as a chemical micro sensor to detect and speciate electroactive ions in solution [17].

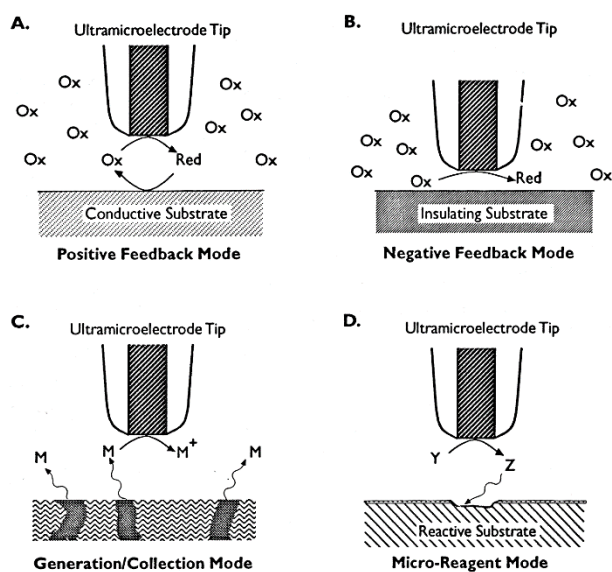


Figure 2. Diagrams of the modes of operation of the scanning electrochemical microscope.

A unique advantage of the SECM is that, if desired, the mediator can be designed to interact with the substrate surface to provide chemical and electrochemical information at micron and submicron resolution. In addition, the SECM can be used to perform local modification of a surface by electrogenerating a chemical reagent at the SECM tip (Figure 2D). This capability has been used to etch metals and semiconductors and to deposit metals [15] as well as derivatizing surface amine groups [18].

This paper describes several experiments in which the SECM is used to study pitting corrosion process. Imaging of an active corrosion pit with the g/c mode of the SECM shows a heterogeneous distribution of oxidizable chemical species in the solution near and at the corrosion pit. In addition, I show

that the SECM can be used to initiate a single corrosion pit on bulk stainless steel and aluminum surfaces by electrogeneration of a local concentration of Cl^- ions.

Experimental Section

Reagents

Trichloroacetic acid (Aldrich) and all other chemicals were reagent grade and were used as received. All solutions were made with 18 M Ω water (Milli-Q, Millipore Corp.) and solution pH was adjusted with HCl or KOH as necessary.

Electrodes

Ultramicroelectrode tips were prepared by sealing Au wires of 0.1 and 0.0127-mm dia. (Aeser Johnson Matthey, Ward Hill PA) as described previously [19]. All tips were polished with successive grades of alumina on cloth down to 0.05 μm to provide a smooth surface with nanometer scale roughness. Amalgamated Au tips were prepared by dipping a gold electrode into triply distilled Hg, removing the tip and allowing the amalgamation to proceed for 24 hours. The amalgamated tips were then polished with 0.05 μm dia. alumina on cloth prior to use.

Metal substrates were prepared by potting the metal samples in EPON 828 epoxy (gift of Shell Chemical Corp., Houston TX) with triethylenetetramine hardener (Miller-Stephensen, Danbury CT). After curing, the samples were exposed by wet grinding with successive grades of 240, 400, and 1000 grit silicon carbide paper. Final polishing was with 6.0 and 1.0 μm diamond polish on nylon cloth followed by 0.05 μm alumina on cloth. Between and after each polishing stage, the electrodes were sonicated in methanol for a minimum of 5 min. The aluminum electrodes were prepared from 1.0 mm dia. annealed Al wire (99.999%, Aeser). Stainless steel samples were prepared from 0.5 mm thick AISI 304 foil (18% Cr, 10% Ni, Goodfellow Corp., Malvern, PA) such that the exposed electrode was in the shape of a band about 2 cm long by 0.5 mm wide.

Potentials were recorded versus a Ag/AgCl reference electrode with a porous Vycor junction. The auxiliary electrode was Pt gauze or wire.

Experimental Apparatus

The SECM used is similar to previously published designs (Figure 1) [19]. The tip electrode is mounted on a 3-axis translation stage that uses piezoelectric inchworms and a model 6000 controller (Burleigh Instruments, Inc., Fishers, NY) to effect submicrometer movements. Position, axis, and velocity control of the stage are provided by TTL signals from a CTM-05 counter-timer board (Keithley Metrabyte, Taunton, MA). Each TTL pulse edge causes a small movement (about 5 nm). Exact control of the tip movement is possible by varying the number and frequency of the pulses. Calibration of the tip movement as a function of axis and velocity was accomplished by measuring the total distance moved after a large number of pulses.

A bipotentiostat (EI-400, Enscan Instruments, Bloomington IN) permitted simultaneous potential control of the tip and substrate electrode and the computer-controlled data acquisition allowed simultaneous acquisition and storage of tip and substrate currents.

The electrochemical cell for the SECM consists of a Teflon cup with a hole in the bottom into which the substrate electrodes could be press fitted. The cell was mounted such that the tip was directly above the substrate electrode.

Results and Discussion

SECM Imaging of Active Pitting Corrosion.

An SECM image of an active corrosion pit on 304 SS is shown in Figure 3. This image was acquired in the generation/collection (g/c) mode at a 12.5 μm dia. Au tip scanning above the substrate surface at a separation of about 20 μm at a scan rate of 40 $\mu\text{m/s}$. The steel sample was biased at +0.5 V vs. an Ag/AgCl reference electrode in a solution containing 10 mM total Cl^- ion at pH 3.0. The SECM image was made by biasing the tip to +1.0 V and rastering it over the corrosion pit. The image thus acquired is a map of the distribution of oxidizable corrosion products emanating from the corrosion pit. The image in Figure 3 is shown in a gray scale format where the tip current intensity is mapped as shades of gray onto a two-dimensional grid with larger anodic currents represented as lighter shades. The pit is about 120 μm in diameter and is located in the upper right side of the image. An interesting aspect of the image is the

extremely heterogeneous current distribution. In addition to one large area of high tip current, several smaller areas with high and intermediate current flow are seen.

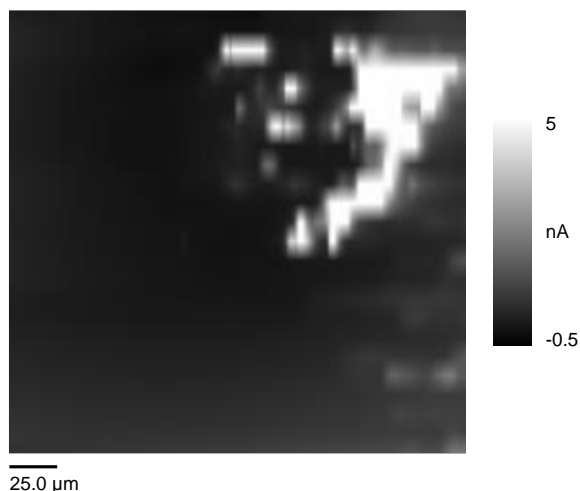


Figure 3. A gray-scale SECM image ($230 \times 230 \mu\text{m}$) of an active corrosion pit on 304 SS. The image was acquired with a $12.5 \mu\text{m}$ diam. Au tip biased at $+1.0 \text{ V}$ vs. Ag/AgCl scanning above the substrate surface at a separation of about $20 \mu\text{m}$ at a scan rate of $40 \mu\text{m/s}$. The steel sample was biased at $+0.5 \text{ V}$ in a solution containing 10 mM total Cl^- ion at pH 3.0.

This heterogeneous current distribution suggests that corrosion products are not being generated uniformly within the pit interior, suggesting in turn that corrosion is not occurring uniformly. Perhaps the most interesting features are the small regions of high tip current. The size of these spots are approximately that of the tip size ($12.5 \mu\text{m}$). Since the size of the tip governs the image resolution, it is likely that the source of these features is smaller than the tip size. An estimate of the concentration of oxidizable species responsible for the tip current can be made from the relationship for the steady-state current at an ultramicroelectrode disk electrode [20].

$$i = 4rnFDC \quad (1)$$

Where r is the electrode radius, F is the Faraday, D is the diffusion coefficient, and C is the concentration. Assuming a single electron transfer and $D = 1 \times 10^{-5} \text{ cm}^2 \text{ s}^{-1}$, the maximum concentration observed here is approximately 2 mM . Note, however, that the maximum current observed was limited by the current transducer so in fact higher concentrations were likely present.

One of the advantages to the use of the SECM is that the scanning probe can also be used as a voltammetric sensor. Figure 4 shows a cyclic voltammogram taken while the tip was positioned close to the

corrosion pit. The broad voltammetric wave has a half-wave potential of 0.86 V vs. Ag/AgCl. The most likely redox couple is, of course, the Fe(II)/Fe(III) system, although the wave is slightly positive of the reversible position for this wave. This suggests that most of the anodic current mapped by the SECM image is due to Fe(II) oxidation.

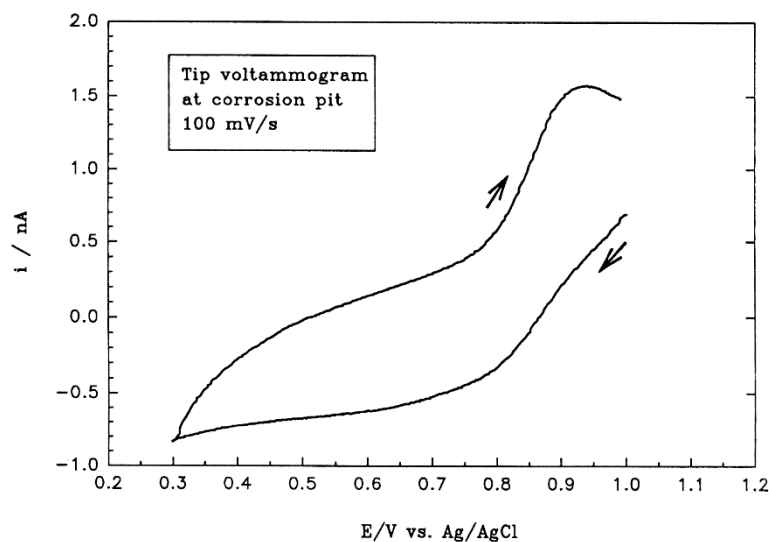
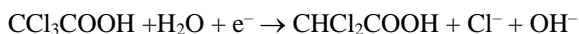


Figure 4. Tip voltammogram acquired near the active corrosion pit shown in figure 3.

Pit Initiation on Stainless Steel with the SECM

By using the SECM tip to electrogenerate Cl^- ions it should be possible to initiate pitting corrosion near the SECM tip. Use of small tips will limit the amount of Cl^- generated and additionally, will confine an effective concentration near a small volume near the tip. In order to demonstrate this capability of the SECM instrument, an attempt was made to generate single corrosion pits on stainless steel.

The general scheme used for the chloride generation is to reduce a water-soluble organic halide added to the electrolyte solution. Many organic halides are unstable upon reduction and decompose to form Cl^- and a radical fragment (Figure 1) [21]. For this study, trichloroacetic acid, CCl_3COOH (TCA) was chosen for its solubility and moderate reduction potential. TCA is reduced via 3 one-electron steps to yield acetic acid. In this case, only the first reduction was of interest:



$E_{1/2}$ for the irreversible wave is reported to be -0.894 V vs. SCE at pH 3.98 [22]. Biasing the SECM tip at potentials more negative than this should quantitatively generate Cl^- from the TCA precursor.

Figure 5 shows a current–time trace in which a corrosion pit was initiated with Cl^- generation. The electrolyte solution in this experiment was 30 mM of TCA. Since TCA is a strong acid ($\text{pK}_a = 0.69$), KOH was added to adjust the pH of the solution to 2.4. The steel substrate was 304 SS and the tip was a 50 μm radius Au amalgam electrode positioned about 100 μm away from the substrate. Before time zero in Figure 5, the substrate potential was adjusted to 0.6 V vs. Ag/AgCl. Shortly after time zero, the tip potential was adjusted to -1.1 V, and a cathodic current of 720 nA due to reduction of TCA at the tip is recorded. The use of amalgamated tips avoids the complication of hydrogen ion reduction at this potential. At a time of 720 s, the steel bias potential was increased to +0.8 V. After an additional 500 s a fluctuation in the current at the steel substrate is seen. Nearly coincident with the current fluctuations at the substrate, the tip current shows an increase in cathodic current. At 1400 s a large current spike is observed at the steel substrate. Accompanying this pulse, the current on the tip fluctuates and then saturates at 1 μA , the current–limit of the transducer.

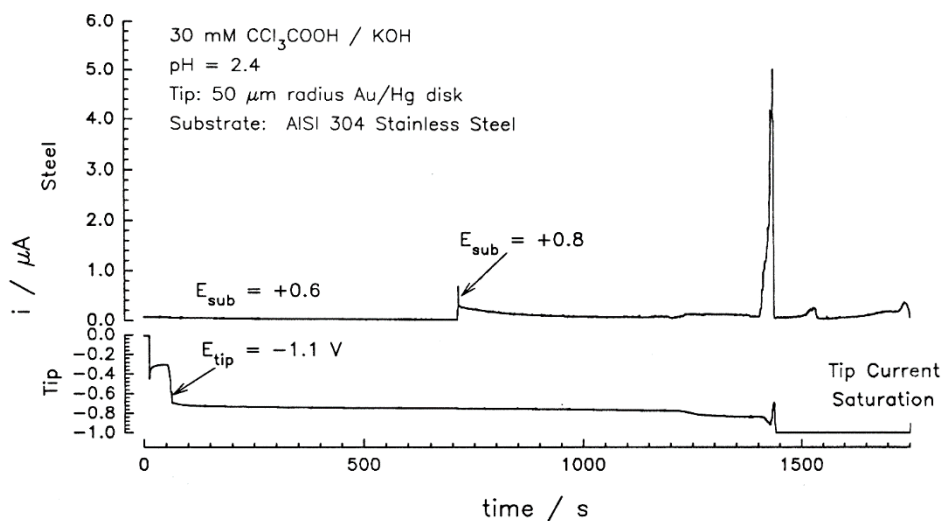


Figure 5. Current–time traces at the tip and steel substrate during an SECM–initiated corrosion pit event. Conditions: 30 mM trichloroacetic acid adjusted to pH 2.4 with KOH. Tip is a 50– μm radius Au amalgam disk electrode positioned about 100 μm from the steel surface. Cl^- generation at the tip occurs when the tip is biased to -1.1 V vs Ag/AgCl. The steel potential was set for 0.6 and then 0.8 V during the course of the experiment.

The current spike observed at the steel substrate is consistent with initiation, growth, and repassivation of a single corrosion pit [8]. Figure 6 shows a current–time graph for the same electrode with 10 mM of Cl^- present in the bulk solution. In this solution and at a potential of 0.3 V, stable (that is, continuously growing) pits are not observed, but many small pits are nucleated, grow, and then repassivate. As observed, the slow rise during the growth phase, and the sharp current drop with passivation is characteristic of unstable pit formation [7–8]. Note that the shape of the current spike in Figure 5 is qualitatively similar to the largest spike in Figure 6. In addition, optical microscopic examination of the region of the steel surface located where the SECM had been generating Cl^- showed a small corrosion pit of dimension $15 \times 20 \mu\text{m}$. A rough calculation of the volume of material removed during the pitting event of Figure 5, based on $90 \mu\text{C}$ of charge passed during the spike, gives a cube of material $16 \mu\text{m}$ on a side, in good agreement with the observed microscopic size.

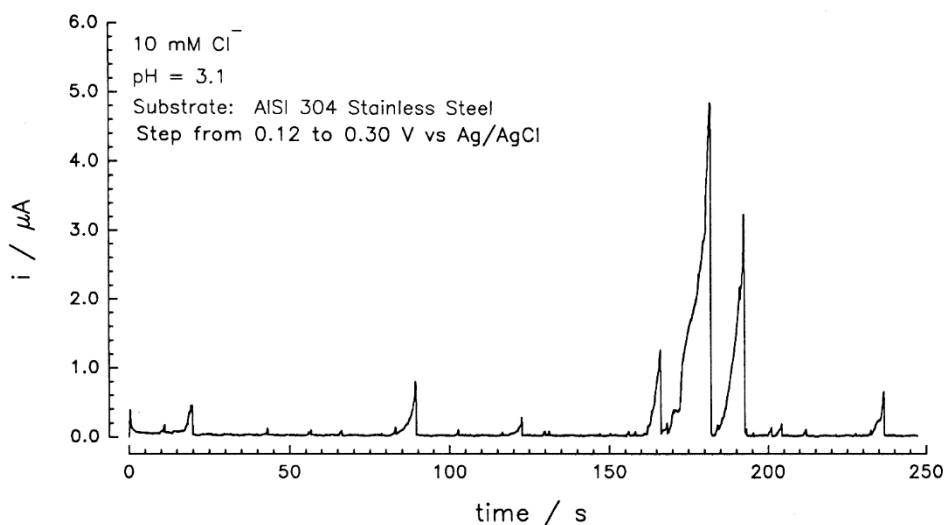


Figure 6. Current–time trace for the 304 SS electrode in a pH 3.1 solution containing 10 mM Cl^- . At time zero the potential was stepped from the rest potential of 0.12 V to 0.3 V vs Ag/AgCl.

Figure 7 is an expanded view of the pit initiation region of Figure 5. This shows that the substrate pit location must be physically close to the site of Cl^- generation. The 60 nA current increase at the steel electrode 200 s before the pit formation is matched by a 50 nA cathodic current increase at the tip electrode. This suggests the oxidizable species dissolving from the sample are being reduced at the tip, with

the implication that the source of the oxidized species is close to the tip location. At this point, the identity of the species being reduced at the tip is unknown, although Fe(II) seems the most likely candidate. A further increase in current occurs at the pitting current spike. It is unclear why the current decreases and then increases to saturation as the pit re-passivates. A speculative explanation for the current increase after the pitting event is increased hydrogen ion reduction catalyzed by metal deposited on the tip electrode.

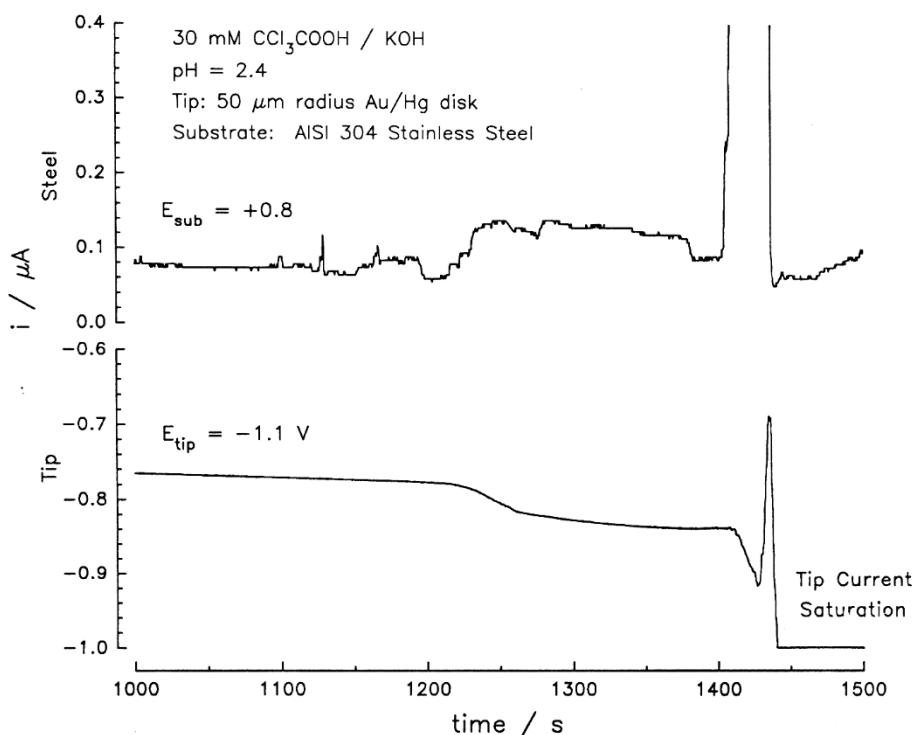


Figure 7. Expanded current–time trace of Figure 5.

A second attempt at pit generation is shown in Figure 8. This attempt was made under similar conditions to those of Figure 5. In this situation the tip was poised to produce Cl^- and again current fluctuations at the substrate were observed along with an increase in the cathodic current at the tip. This suggests again that the oxidized products of the steel dissolution were formed near the tip electrode. In contrast to the data in Figure 5, no single current spike corresponding to a single pitting event is observed. At a time of 750 s the Cl^- generation was interrupted, at this point the current at the steel substrate immediately dropped to baseline levels. Optical microscopic examination of the steel surface after this

attempt at pit generation did not show a single pit, but instead a group of small pits with diameters of 1–5 μm clustered within a 30 μm dia. region.

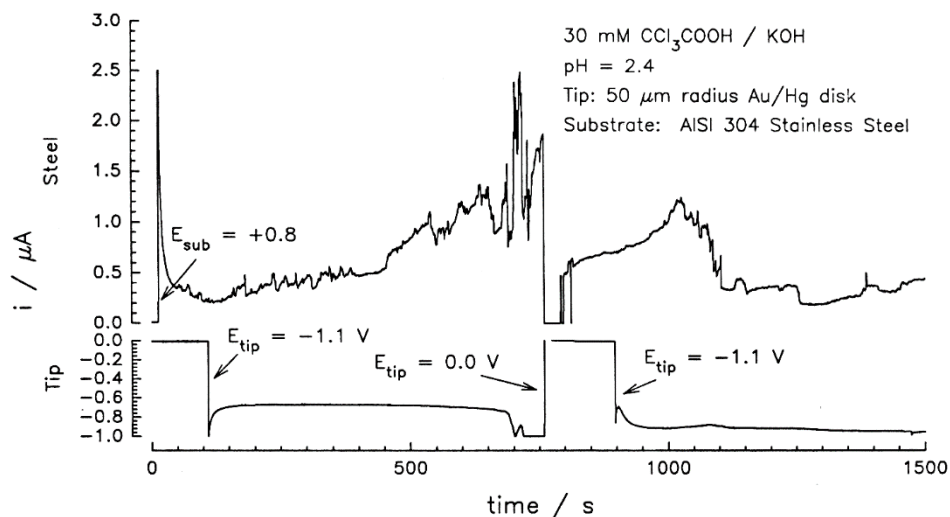


Figure 8. An additional set of current time traces for the pit initiation experiment. Conditions are identical to those in Figure 5 but with the tip moved to a position about 1 cm distant from the pit initiated in Figure 5. The tip–steel separation was about 100 μm .

The data in figures 5 through 8 raise a question. For both SECM initiated pit nucleation events, about 700 s transpire after application of 0.8 V and tip Cl^- generation. Why is there such a long induction time for pit formation with localized Cl^- generation? This is in contrast to the situation where pits form nearly instantaneously when Cl^- is present in the bulk solution and the steel is held at a potential of 0.8 V. One aspect of this is the small size of the region undergoing pitting. For the conditions here, generation of about 30 mM Cl^- at a 100 μm dia. tip, a region of the steel surface approximately 200 μm in diameter would be expected to be exposed to Cl^- concentrations higher than 10 mM. 1 pit every 700 s leads to a nucleation frequency of about $4.5 \text{ cm}^{-2} \text{ s}^{-1}$. In contrast, the pit nucleation frequency for the data in Figure 6, at a substrate potential of +0.3 V and 10 mM Cl^- , is about $0.3 \text{ cm}^{-2} \text{ s}^{-1}$. Although the limited data makes quantitative assessment impossible, the nucleation frequency for the SECM initiated experiments is at least roughly similar to the frequency when bulk Cl^- is present, suggesting that there is not a qualitative difference in the initiation process between the two methods.

Pit Initiation on Aluminum with the SECM

Initiation of pits on high purity aluminum was also attempted. Figure 9 shows a current–time trace for SECM–initiated pitting. Conditions for this experiment are essentially identical to conditions for the stainless–steel pitting experiment. The aluminum substrate was high purity wire (1 mm dia., 99.999% Al) held at a potential of -0.2 V. At a time of about 100 s after initiation of Cl^- generation at the tip, a large pulse of substrate current (sufficient to saturate the current transducer) was observed. This was accompanied by fluctuations in the tip current. This large current persisted for about 75 s and then fell to a level of about $18 \mu\text{A}$. This current persisted and grew to a magnitude of greater than $50 \mu\text{A}$ over a period of 800 s. Attempts to return the current to pre-pitting levels by stopping Cl^- generation at a time of 240 s and 900 s were unsuccessful. Bubble formation at the Al surface was observed during the time the current–time trace was recorded. In addition, the pit grew large enough to be visible during the course of the experiment. The oscillations at the tip and substrate are likely due to the bubble formation process. Note that here, unlike in the steel experiment, no increase in tip current is observed upon pitting, since the Al(III) ion is not electroactive at the tip potential.

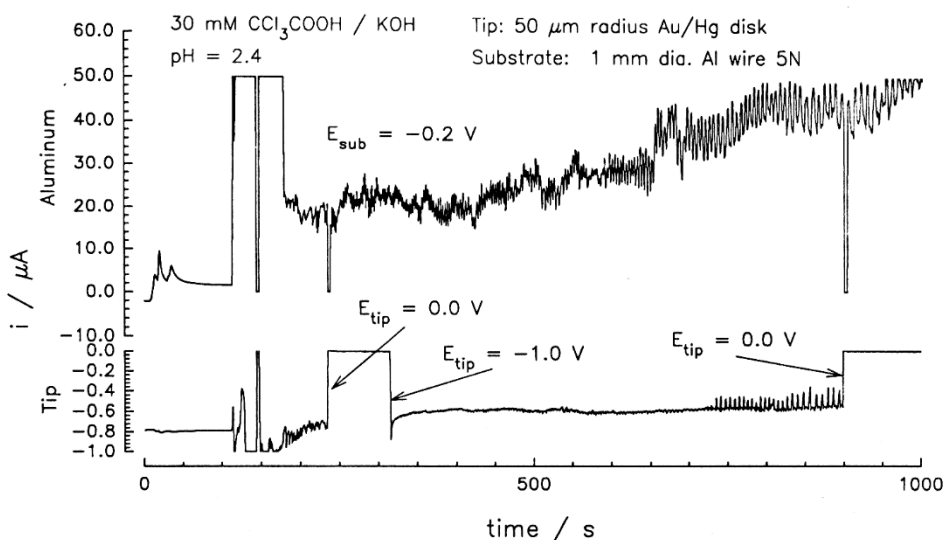


Figure 9. Current–time traces at the tip and high–purity Al (99.999%) substrate during an SECM–initiated corrosion pit event. Conditions: 30 mM trichloroacetic acid adjusted to pH 2.4 with KOH. Tip is a 50 μm radius Au amalgam disk electrode positioned about 100 μm from the Al surface. Cl^- generation at the tip occurs when the tip is biased to -1.0 V vs Ag/AgCl . The Al electrode was biased at -0.2 V during the course of the experiment.

Examination of the Al surface by optical microscopy showed 2 large pits: one pit of $100 \times 200 \mu\text{m}$ and another of about $60 \times 100 \mu\text{m}$ at the edge of the Al disk. The interior of these pits showed numerous rectangular crystallites $2\text{--}3 \mu\text{m}$ in size.

For these experiments it is not clear if the pit initiation was triggered by the SECM-generated Cl^- , since at this pH, the corrosion rate of Al is large. Once initiated, the free corrosion that occurred to enlarge the pits was certainly due to the low pH conditions. However, the formation of the initial pitting seems to be linked with the Cl^- generation at the SECM tip.

Conclusions

The preliminary results presented here demonstrate that SECM can be a useful tool for the examination of corrosion process. Future work will examine SECM-initiated pitting as a function of pH, substrate potential, and Cl^- concentration. The use of generated Cl^- and other aggressive anions will allow examination of pit nucleation at very positive potentials, where pit nucleation processes in the presence of bulk Cl^- are obscured by the large number of corrosion pits and the subsequent large background current. In addition, g/c mode SECM will also be used to image the initiated pit to examine the rate of growth and corrosion products. Use of smaller tips will allow greater spatial resolution. Also, experiments are planned in which imaging in the feedback mode is used to preselect sites for pit initiation. In this way, pitting processes can be examined as a function of surface heterogeneity. For example, pit initiation is expected to require lower bias potentials and shorter induction times at scratches and sulfide inclusions than at undisturbed metal.

Acknowledgment

I wish to thank Robert C. Tenent for his contribution to this work and Thomas P. Moffat for suggesting the investigation of pitting corrosion with SECM. This work is supported in part by the NSF EPSCoR Program (Grant EHR 91-08767), The State of Mississippi, and Mississippi State University. Additional support by MSU Office of Research and by the Petroleum Research Fund is gratefully acknowledged.

References

1. H. Kaesche, *Metallic Corrosion*, NACE, Houston TX, 1985 and references therein.
2. N. Sato and G. Okamoto in J. O'M. Bockris, et al. (Eds.), *Comprehensive Treatise of Electrochemistry*, Plenum Press, New York, 1981, p. 193.
3. Z. Szklarska-Smialowska, *Pitting Corrosion of Metals*, NACE, Houston TX, 1986
4. H.-H. Strehblow in *Proceedings of the 9th International Congress on Metallic Corrosion*, NRC, Toronto, Canada, 1984, p. 99.
5. T. P. Hoar, D. C. Mears and G. P. Rothwell, *Corros. Sci.*, 5 (1965) 279.
6. T. P. Hoar and W. R. Jacob, *Nature*, 216 (1967) 1299.
7. D. E. Williams, C. Westcott and M. Fleischmann, *J. Electrochem. Soc.*, 132 (1985) 1796.
8. D. E. Williams, C. Westcott and M. Fleischmann, *J. Electrochem. Soc.*, 132 (1985) 1804.
9. H. S. Isaacs and B. Vyas in F. Mansfeld and U. Bertocci (Eds.), *Electrochemical Corrosion Testing*, STP 727, American Society for Testing and Materials, 1981, p. 3.
10. H. S. Isaacs, *Corros. Sci.*, 29 (1989) 313.
11. D. E. Williams in M. I. Montenegro, et al. (Eds.), *Microelectrodes: Theory and Applications*, Kluwer Academic Publishers, Boston, 1991, p. 445-451.
12. G. Binnig and H. Rohrer, *Helv. Phys. Acta*, 55 (1982) 726.
13. G. Binnig, C. Quate and C. Gerber, *Phys. Rev. Lett.*, 56 (1986) 930.
14. A. J. Bard, F.-R. Fan, J. Kwak and O. Lev, *Anal. Chem.*, 61 (1989) 132.
15. A. J. Bard, G. Denuault, C. M. Lee, D. Mandler and D. O. Wipf, *Acc. Chem. Res.*, 23 (1990) 357.
16. A. J. Bard, F.-R. Fan, D. T. Pierce P. R. Unwin, D. O. Wipf, and F. Zhou, *Science*, 254 (1991) 68.
17. R. C. Engstrom, T. Meany, R. Tople and R. M. Wightman, *Anal. Chem.*, 59 (1987) 2005.
18. R. C. Engstrom, C. R. Dick, D. L. Fritza and M. D. Koppang, Pittsburgh Conference and Exhibition, Atlanta, GA, 1993, Abstract #060.
19. D. O. Wipf and A. J. Bard, *J. Electrochem. Soc.*, 138 (1991) 469.
20. R. M. Wightman and D. O. Wipf in A. J. Bard (Ed.), *Electroanalytical Chemistry*, Vol. 15, Marcel Dekker, New York, 1989, p 267-355.
21. M. D. Hawley in A. J. Bard and H. Lund, (Eds.), *Encyclopedia of Electrochemistry of the Elements*, Marcel Dekker, New York, 1980. p 1-238.
22. P. J. Elving and C.-S. Tang, *J. Am. Chem. Soc.*, 72 (1950) 3244 .